Electronic Supplementary Material (ESI) for Physical Chemistry Chemical Physics.

Electronic Supplementary Information for "Distinct Molecular Dynamics Dividing Liquid-Like and Gas-Like Supercritical Hydrogens"

Shutaro Yamaoka and Kim Hyeon-Deuk*

Department of Chemistry, Kyoto University, Kyoto, 606-8502, Japan

E-mail: kim@kuchem.kyoto-u.ac.jp,Phone:+81-75-753-4021

*To whom correspondence should be addressed

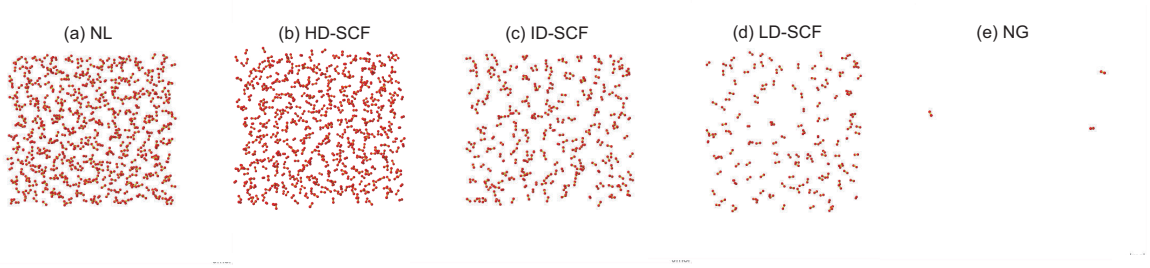

Figure S1: Snapshots of the cubic simulation boxes of the (a) normal liquid (NL), (b) high-density supercritical fluid (HD-SCF), (c) intermediate-density supercritical fluid (ID-SCF), (d) low-density supercritical fluid (LD-SCF), and (e) normal gas (NG). Because we matched the box size visualized here, the number of H_2 molecules contained in each box is different depending on the density. The actual simulations were all performed for 640 H_2 molecules by changing the total box volume.

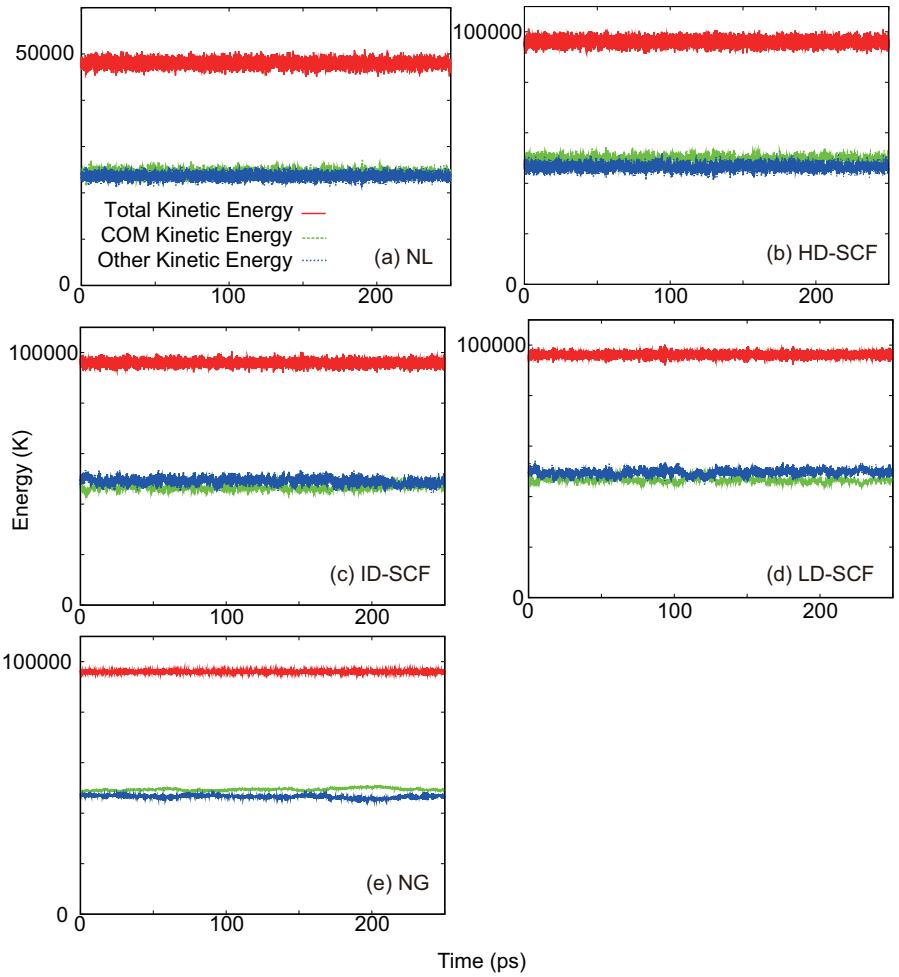

Figure S2: Total kinetic energy, kinetic energy of the centers of mass (COM), and the other kinetic energy in the (a) NL, (b) HD-SCF, (c) ID-SCF, (d) LD-SCF, and (e) NG. The equipartition between the kinetic energy of the COM and the rest is well attained.

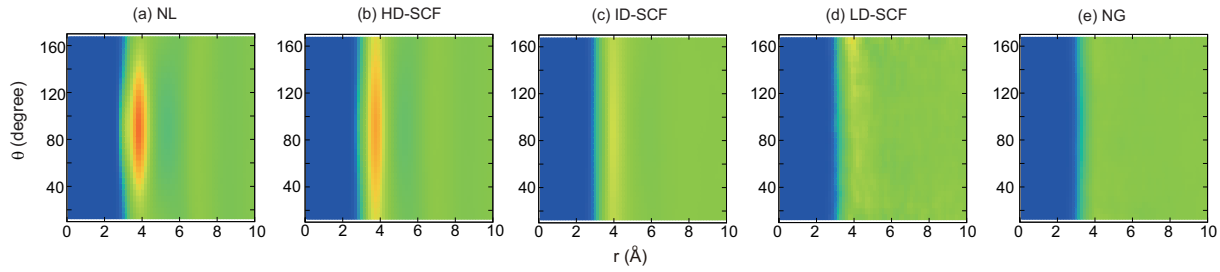

Figure S3: Two-dimensional (2D) radial distribution functions (RDFs) of the (a) NL, (b) HD-SCF, (c) ID-SCF, (d) LD-SCF, and (e) NG as a 2D function of the radial distance r and relative molar angle θ. The 2D RDF,

$$g(r,\theta) = \frac{\langle n(r,\theta)\rangle}{2\pi n_0 r^2 dr \sin\theta d\theta},$$

is defined as a 2D function of the radial distance between nuclear wave packet (NWP) centers, r, and the relative molar angle of an H_2 pair, θ. Here, $n(r,\theta)$ represents the number of NWPs within a small region of radii $r \sim r + dr$ and angle $\theta \sim \theta + d\theta$. The 2D RDFs become flatter along r and θ as the temperature and density become higher and lower, respectively; the first peak of the 2D RDF becomes smaller and the periodicity of the peaks and valleys becomes less enhanced from the left NL case to the right NG cases. The main peak appearing around $\theta = 90$ degrees in the first peak of the NL 2D RDF indicates a T-shape first solvation shell stably formed in the NL. It should be mentioned that, although the most stable solvation structure is a T-shape, other configurations are also possible as can be seen in the broad first peak of the 2D RDF along θ. Actually, the first peak of the 2D RDF along θ is much broader in the HD-SCF than in the NL, indicating that the higher temperature induced the more broken and fragile T-shape shell in the HD-SCF despite the same density as discussed in Fig.1. The change of the 2D RDFs depending on the thermodynamic points shown here

directly reflects the effective potential change depending on the temperature and density because a 2D RDF directly reflects an intermolecular potential at a given thermodynamic point.

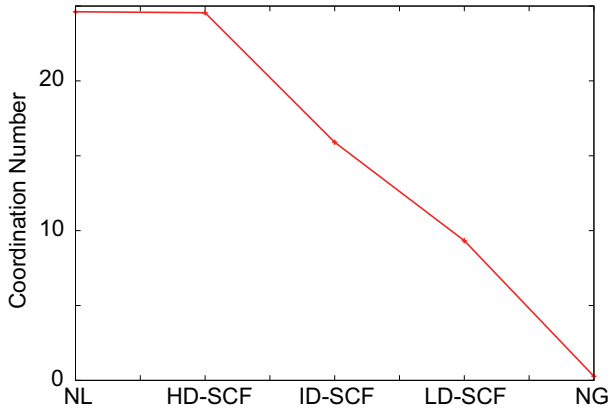

Figure S4: Coordination number in the first solvation shell. The calculated coordination number monotonically decreases in the order of the NL, HD-SCF, ID-SCF, LD-SCF, and NG. Especially, the coordination number of the NG is almost zero, being consistent with its almost flat RDF without a clear first peak.

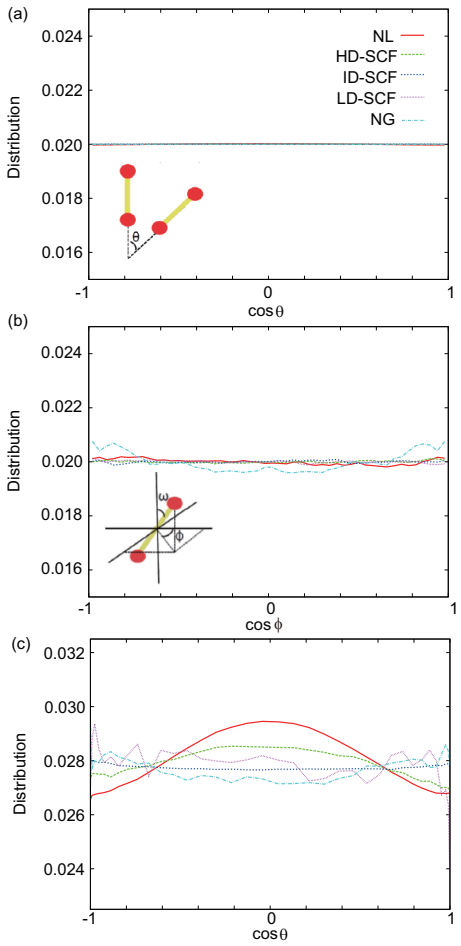

Figure S5: Distributions of (a) the relative molar angle θ, (b) the self-orientational angle ϕ defined as a molecular angle projected on the xy-plane, and (c) the relative molar angle θ for molecular pairs whose intermolecular center of mass distance is smaller than the first valley position of the corresponding RDF shown in Fig.1. The distribution of the relative molar angle θ shown in Fig.S5(a) is not perfectly linear but almost linear. It is more linear than the distribution of the self-orientational angle ϕ shown in Fig.S5(b) because the number of samples to calculate the former is much larger than the latter due to a huge number of combination of paired molecules and the statistical accuracy is more warranted in the former

than in the latter. In Fig.S5(c), the clear peak appears around θ=90 degrees in the NL and HD-SCF while such peak cannot be seen in the ID-SCF, LD-SCF and NG, which is in harmony with the 2D RDFs discussed in Fig.S3. The clear peak appearing around θ=90 degrees demonstrates the T-shape first solvation shell stably formed in the NL and HD-SCF. Note that the LD-SCF and NG distributions fluctuate due to a small number of molecules included within the first valley position of the RDF.

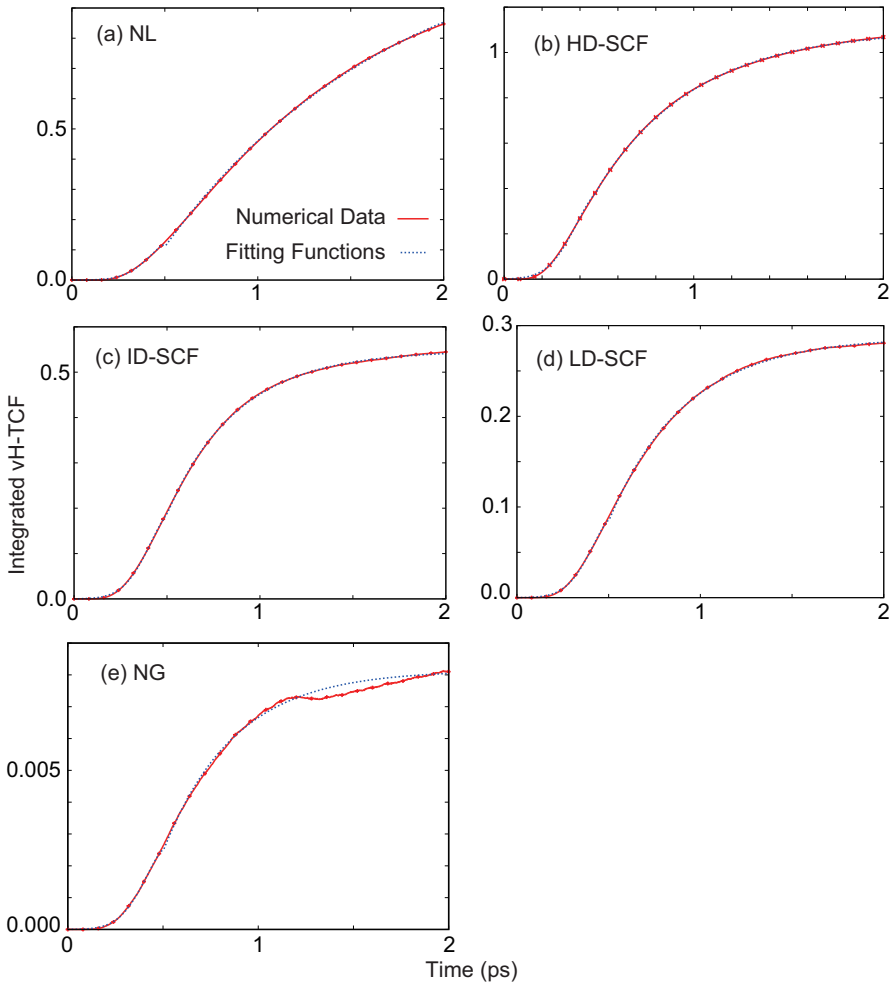

Figure S6: Time evolution of the integrated area of the van Hove time correlation functions (vH-TCFs) displayed in Figs.2(a)-2(e) for $r < 2$Å where the translational smearing dynamics of hydrogen molecules most significantly appears. Each time-dependent integrated area was almost completely fitted by the Gaussian function within the initial 0.5 ps and by the single exponential function after 0.5 ps. (See Tables S1 and S2) The small standard error bars guarantee that the time evolution of the integrated area of the vH-TCFs is well converged, and thus that their fitting functions and fitting parameters listed in Tables S1 and S3 are also well converged within the small standard error bars. Note that Fig.2(f)

simply shows the fitting parameter e_2 in Table S2. The present small error bars can be achieved owing to a huge number of samples which the nuclear and electron wave packet molecular dynamics (NEWPMD) method can provide, i.e. real-time 300 ps trajectories of 640 H_2 molecules.

	G_0	G_1	G_2
NL	0.14095	576.67	205.26
HD-SCF	0.40212	534.65	215.59
ID-SCF	0.20485	563.44	211.73
LD-SCF	0.09611	566.98	210.34
NG	0.00282	565.99	209.25

Table S1: Fitting parameters G for the Gaussian function $G_0 \exp(-(t - G_1)^2/G_2^2)$ used in Fig.S6.

	e_0	e_1	e_2	e_3
NL	-1.04792	521.26	1255.2	1.1759
HD-SCF	-0.80316	423.78	522.31	1.1028
ID-SCF	-0.71427	241.16	378.93	0.5480
LD-SCF	-0.37743	239.11	420.59	0.2875
NG	-0.01176	229.83	372.59	0.0081

Table S2: Fitting parameters e for the exponential function $e_0 \exp(-(t-e_1)/e_2)+e_3$ used in Fig.S6.

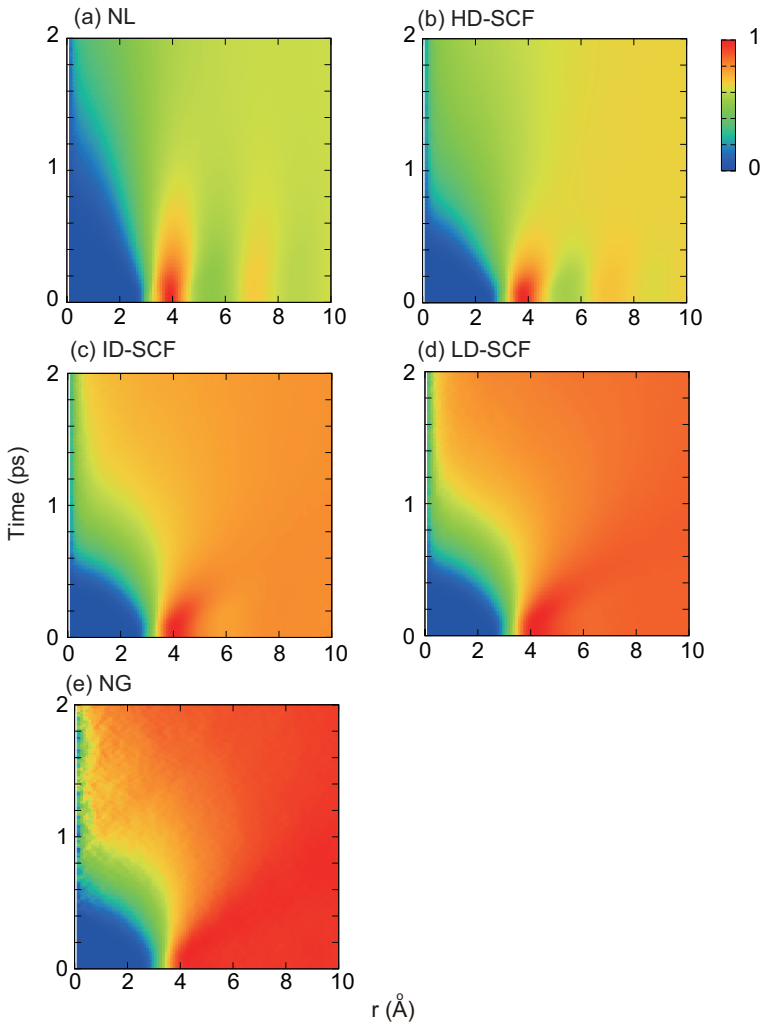

Figure S7: 2D vH-TCFs $G(r,t)$ defined in eq.(1) as a 2D function of time and the radial distance r for the (a) NL, (b) HD-SCF, (c) ID-SCF, (d) LD-SCF, and (e) NG. Each 2D vH-TCF was normalized by the maximum value. The 2D vH-TCFs behave similar to the vH-TCFs shown in Fig.2. The 2D vH-TCF is linked to the stiffness of the solvation structure and supports our insights on the stability of the solvation shells depending on the density and temperature discussed in Fig.1. The initial hole part of the 2D vH-TCF shown as the blue region becomes filled with time, and the initial oscillative correlation of the structure

finally disappears. It can be seen that the blue-colored empty area of the 2D vH-TCF is smaller in the ID-SCF than in the LD-SCF, indicating the faster time evolution of the former than the latter.

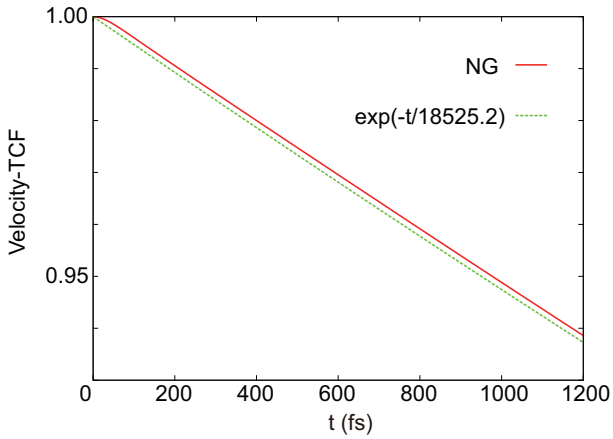

Figure S8: TCF of the center of mass velocity $\mathbf{V}(t)$ for the NG, $\langle \mathbf{V}(t) \cdot \mathbf{V}(0) \rangle$ scaled by the initial value at $t = 0$. The calculated velocity-TCF was well fitted by the single exponential function, $\exp(-t/19498.8)$. The self-diffusion coefficient for the NG can be calculated as $\int_0^\infty dt \langle \mathbf{V}(t) \cdot \mathbf{V}(0) \rangle$.

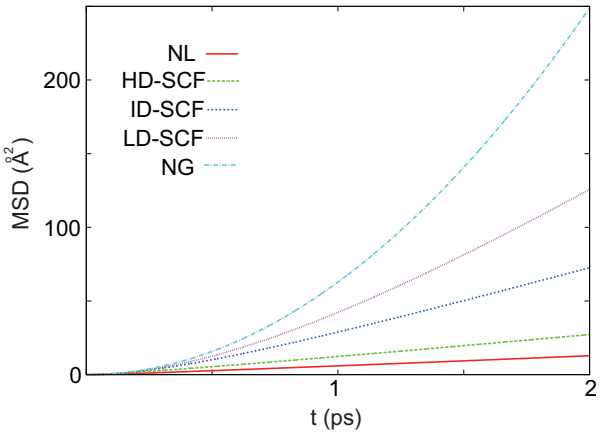

Figure S9: Initial mean square displacements of the NL, HD-SCF, ID-SCF, LD-SCF, and NG as a function of time t.

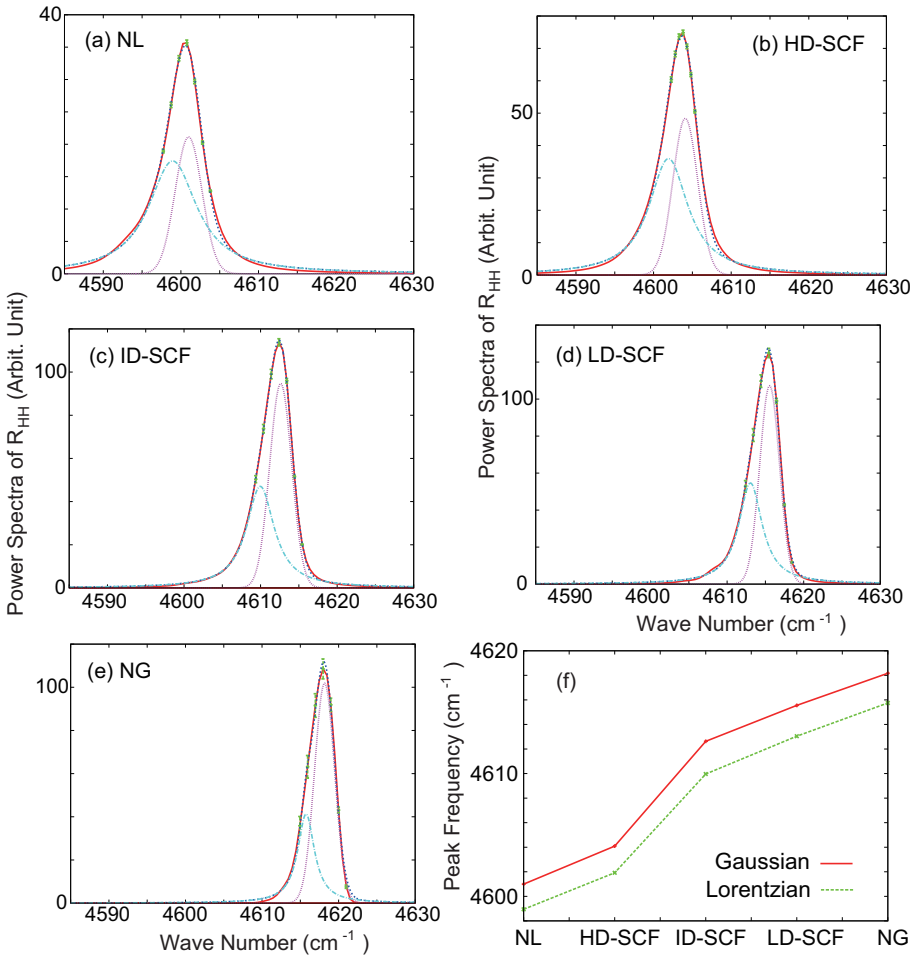

Figure S10: Power spectra of $R_{HH}(t)$ in the (a) NL, (b) HD-SCF, (c) ID-SCF, (d) LD-SCF, and (e) NG (red lines) with the standard error bars (green vertical bars), and (f) their split peak frequencies. The standard error bars demonstrate that the power spectra are converged within the current resolution of the power spectra, 0.5 cm^{-1}. These small error bars were achieved owing to a huge number of samples which the NEWPMD method can provide, i.e. real-time 300 ps trajectories of 640 H_2 molecules. The vibrational power spectra can be almost perfectly fitted with a sum of the two split functions (blue lines), the Gaussian function $a_0 \exp[-(x-a_1)^2/a_2^2]$ (purple lines) and the Lorentzian function $a_0/((x-$

$a_1)^2 + a_2$) (light-blue lines) whose parameters are listed in Table S3. The peak frequencies, a_1 shown in Fig.S10(f), are red-shifted in the order of the NL, HD-SCF, ID-SCF, LD-SCF, and NG regardless of the fitting functions. We had tried various kinds of fitting, and finally found that the current combination of the single Lorentzian and single Gaussian functions is the best fit. For fitting, we used the program called scipy.optimize.curve_fit provided by Python, and then manually adjusted the parameters to get the best fitting. Physically, the Lorentzian function indicates the existence of the motional narrowing while the Gaussian function reflects inhomogeneous vibration. The convergence of the power spectra and their well-fitting assure the convergence of Fig4(b). We note that, because the deviation of the peak frequency shown in Fig.4(b) is the difference between the two fitting parameters a_1 listed in Table S3, the standard error bars cannot be directly given to Fig.4(b).

Fitting Functions	a_0	a_1	a_2
Gaussian (NL)	2111.6	4600.993	2.45
Gaussian (HD-SCF)	4835.0	4604.087	2.27
Gaussian (ID-SCF)	9462.2	4612.627	2.03
Gaussian (LD-SCF)	10720	4615.553	1.82
Gaussian (NG)	10186	4618.169	1.85
Lorentzian (NL)	25195	4598.942	14.5
Lorentzian (HD-SCF)	33667	4601.920	9.37
Lorentzian (ID-SCF)	23133	4609.964	4.92
Lorentzian (LD-SCF)	18971	4613.046	3.47
Lorentzian (NG)	7336.9	4615.751	1.78

Table S3: Fitting parameters for the Gaussian function $a_0 \exp[-(x-a_1)^2/a_2^2]$ and for the Lorentzian function $a_0/((x-a_1)^2+a_2)$ used in Fig.S10. The large difference between a_0 of the Lorentzian function and a_0 of the Gaussian function is simply due to their different function types.

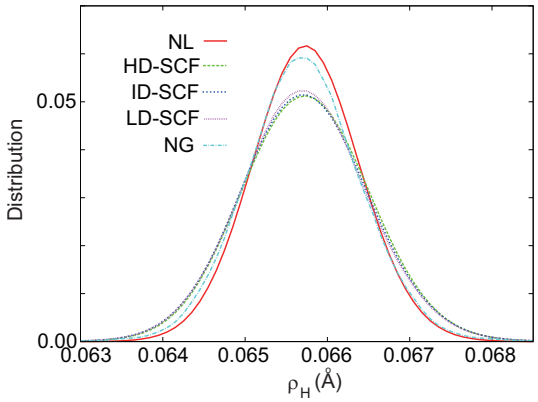

Figure S11: Distribution of the NWP width ρ_{H} for the NL, HD-SCF, ID-SCF, LD-SCF, and NG.